Since January 2020 Elsevier has created a COVID-19 resource centre with free information in English and Mandarin on the novel coronavirus COVID-19. The COVID-19 resource centre is hosted on Elsevier Connect, the company's public news and information website.

Building and Environment 197 (2021) 107852

Contents lists available at ScienceDirect

Building and Environment

journal homepage: http://www.elsevier.com/locate/buildenv

Ultraviolet germicidal irradiation (UVGI) for in-duct airborne bioaerosol disinfection: Review and analysis of design factors

Hao Luo, Lexuan Zhong *

Department of Mechanical Engineering, University of Alberta, 9211-116 Street NW, Edmonton, AB, T6G 1H9, Canada

ARTICLE INFO

Keywords:
Ultraviolet germicidal irradiation (UVGI)
SARS-CoV-2
UV rate constant
Airborne microorganism disinfection
HVAC
Environmental conditions

ABSTRACT

The rapid increase in global cases of COVID-19 illness and death requires the implementation of appropriate and efficient engineering controls to improve indoor air quality. This paper focuses on the use of the ultraviolet germicidal irradiation (UVGI) air purification technology in HVAC ducts, which is particularly applicable to buildings where fully shutting down air recirculation is not feasible. Given the poor understanding of the in-duct UVGI system regarding its working mechanisms, designs, and applications, this review has the following key research objectives:

- Identifying the critical parameters for designing a UVGI system, including the characterization of lamp output, behavior of the target microbial UV dose-response, and evaluation of the inactivation performance and energy consumption.
- Elucidating the effects of environmental factors (air velocity, air temperature, and humidity) on the UVGI system design parameters and optimization of the in-duct UVGI design.
- Summarizing existing UVGI system designs in the literature and illustrating their germicidal and energy performance in light of COVID-19 mitigation.

1. Introduction

The coronavirus disease (COVID-19) pandemic, caused by the severe acute respiratory syndrome coronavirus-2 (SARS-CoV-2), has been global, with over 1.73 million deaths as of December 24, 2020. As a highly contagious human coronavirus, SARS-CoV-2 is mainly transmitted through droplet, contact, and airborne modalities. The short-range droplet-based (large droplets deposited on a surface within 1–2 m) and contact transmission routes have been well recognized and adequate precautions have been implemented, including maintaining a physical distance and washing hands frequently. However, the long-range transmission route in bioaerosols is gaining attention, and mitigating the spread via this route is the most challenging [1–6]. Engineering controls are suggested to introduce fresh outdoor air into the indoor environment, thus preventing airborne contaminant transmission through HVAC systems [7]. However, entirely shutting down recirculation is not feasible in most systems because of the extensive energy consumption required and limited heating/cooling capacities to provide a comfortable indoor environment. Thus, practical recommendations include maximum outdoor air intake and the application of filtering or ultraviolet germicidal irradiation (UVGI) to remove or inactivate potential viral contaminations are proposed [8]. The UVGI system is an effective virus inactivation method that uses short-wave ultraviolet energy (UVC, 200–280 nm) to disinfect viral, bacterial, and fungal organisms by forming photodimers in nucleic acids (DNA and RNA), thus preventing both transcription and replication [9,10]. It has already been recognized and recommended for efficient bioaerosol elimination in HVAC systems [11,12], which account for approximately 27% of the UVGI market [13]. As for the application scenarios, it is reported that its primary installations are in healthcare facilities (60%), whereas office, school, public, and residential buildings account for less than 3% of installations, even though these are major infection locations of contagious respiratory diseases [14,15]. In addition, massive growth in the UV disinfection equipment market is anticipated in the next five years (from USD 4.8 billion to USD 9.2 billion) as a result of the COVID-19 combat [16].

However, the design and optimization of in-duct UVGI systems are poorly understood owing to the limited knowledge of the UV lamp

* Corresponding author.
E-mail address: lexuan.zhong@ualberta.ca (L. Zhong).

https://doi.org/10.1016/j.buildenv.2021.107852
Received 29 December 2020; Received in revised form 11 March 2021; Accepted 29 March 2021
Available online 6 April 2021

output characterization, microbial UV dose-response behavior, inactivation performance in practice, and energy consumption evaluations of UVGI systems. Thus, this paper provides in-depth discussions on the UVGI system fundamentals and performance evaluations. This paper will contribute to our understanding of the mechanisms of the UVGI air purification technology and in-duct UVGI system design and predict its role in the mitigation of COVID-19 transmission.

2. UVGI fundamentals

UVGI uses short-wave ultraviolet energy (UVC) to inactivate viral, bacterial, and fungal organisms, making them unable to replicate themselves and spread diseases. The disinfection performance is commonly quantified as the single-pass inactivation efficacy:

$$\eta = 1 - e^{-kD_{UV}} = 1 - e^{-kIt} \tag{1}$$

where k is the species-dependent microorganism UV rate constant (m^2/J), D_{UV} is the UV dose (J/m^2) delivers to the microorganisms, I is the irradiance (W/m^2), and t is the exposure time (s). The UV dose appears quite simple. However, its application can be complicated (e.g., when calculating the dose received by a microorganism following a tortuous path through a device with spatial variations in irradiance). Further on, three operational factors (air velocity, temperature and relative humidity) are identified critically affecting the in-duct UVGI performance [17–20].

2.1. Germicidal sources

2.1.1. Mercury based UV lamp (low-pressure mercury UV lamp)

Mercury-based UV lamps, which are filled with mercury and a starting gas (typically argon), have a long history in UVGI devices. The commonly used low-pressure mercury germicidal UV lamp has a peak irradiance at 253.7 nm (more than 90% radiative emissions [21]), which is close to the peak germicidal effectiveness wavelength of 265 nm and out of the ozone producing region (<240 nm) [10]. Furthermore, to eliminate ozone generation thoroughly, a soft glass coating is used to filter out the ozone-forming irradiance (185 nm here) and avoid potential ozone hazards in air [22]. The lamp output is another critical design parameter in a UVGI system. Its output is determined by the coldest spot on the lamp surface, which controls the mercury vapor pressure of the lamp. For instance, Philips mercury lamps have optimum UV emitting efficiency (100%) when the bulb wall temperature reaches approximately 40 °C and only 20% and 58% efficiency when the lamp surface temperature is 10 °C and 80 °C, respectively [22]. The temperature dependency leads to concerns for the in-duct UVGI apparatus, as the heat transfer between the lamp and the ambient airflow strongly affects the lamp surface temperature and the lamp output, which is commonly called the "wind-chill" phenomenon. Thus, it is critical to identify the relationship between the HVAC operating conditions and the UV lamp working efficiency (lamp surface temperature). A previous study (Study 1 [23]) introduced empirical correlations of lamp output for three types of low-pressure mercury lamps under common HVAC operating conditions (air temperature: 5–35 °C; air velocity: 0.5–4 m/s). Three lamps, namely, cylindrical hot cathode (type 1), twin-tube hot cathode (type 2), and cylindrical cold cathode (type 3), were placed in the duct, both cross-facing and parallel-facing the airflow. The correlations successfully predicted the lamp output under different air velocity and temperature conditions, where insufficient (low air velocity and high air temperature) or excess (high air velocity and low air temperature) convective heat transfer between the UV lamp and duct airflow results in overheating or overcooling of the lamp, thus lowering its output.

Although the empirical correlations between the lamp outputs and operating conditions of the three types of UV lamps were obtained, extending the conclusions to other lamps (different lamp powers, dimensions, etc.) and flow conditions remains problematic. This paper gathers three peer-reviewed papers to examine their applicability and introduces a universal method for correlating lamp performance with operating conditions and lamp characteristics. The reported lamp performances are organized in Supplementary Material Table S1, categorized by lamp models (type 1 and type 2) and flow characteristics (mixed convection with Richardson number between 0.1 and 10 and forced convection with Richardson number smaller than 0.1). Owing to the different irradiance-measuring locations in the duct, the reported irradiance is not directly comparable. However, discrepancies in the varying trends were observed. For instance, in Studies 1 [23] and 2 [24], where the air temperature increases from 15.5, 20.5–25.5 °C under U = 3 m/s, an increasing and then decreasing lamp irradiance was observed in Study 2 [24], which contradicts the mono-increasing trend observed in Study 1 [23]. For the type 1 lamp, both Studies 1 [23] and 3 [25] reported mono-increasing lamp irradiance with the air temperature varying from 15.5 to 30 °C at U = 3 m/s. Thus, blindly applying case-specific conclusions to broader application scenarios can cause unpredicted discrepancies.

To generalize the correlation between different lamp characteristics and wind-chill effects (i.e., different lamp diameters, lengths, and working powers), this review introduces the concept of the "ratio of convective heat dissipation to radiative heat dissipation" to the heat transfer analytical model in Study 1 [23]. The dimensionless ratio r is written as follows:

$$r = \frac{Q_{conv}}{Q_{rad}} \tag{2}$$

where Q_{conv} and Q_{rad} are the lamp's convective and radiative heat losses, which are calculated by:

$$\begin{aligned} Q_{conv} &= \frac{Nu \cdot k}{D} A (T_s - T_{amb}) \\ Q_{rad} &= \varepsilon A \sigma \left[(T_s + 273)^4 - (T_{amb} + 273)^4 \right] \end{aligned} \tag{3}$$

Nu is the Nusselt number, which has different forms for different flow regimes and lamp shapes. For a cylindrical UV lamp (type 1), the Nusselt numbers of natural and forced convection [23,26,27] are given as:

$$Nu_{N1} = 0.47 (\mathrm{Pr} \cdot Gr)^{1/4} \tag{4a}$$

$$Nu_{F1} = 0.3 + \frac{0.62 \mathrm{Re}^{0.5} \mathrm{Pr}^{1/3}}{\left(0.4/\mathrm{Pr}\right)\left(0.4/\mathrm{Pr}\right)(0.4/\mathrm{Pr})^{2/3}\Big)^{1/4}} \left[1 + \left(\frac{\mathrm{Re}}{282000} \right)^{5/8} \right]^{4/5} \tag{4b}$$

For the twin-tubes UV lamp (type 2), the Nusselt numbers for the natural and forced convections were approximated by the correlation for an ellipse [23,28] as:

$$Nu_{N2} = \frac{1.85}{\ln\left(1 + \frac{1.85}{0.897 C_1 Ra^{1/4}}\right)} \tag{4c}$$

$$Nu = 0.27 \mathrm{Pr}^{0.37} \mathrm{Re}^{0.6} \tag{4d}$$

Based on natural and forced convection, the Nusselt numbers for the mixed convection are obtained by introducing the "effective Reynolds number" (Re_{eff}), which is calculated as the geometric mean of the imaginary Reynolds number (Re_i) for natural convection and real duct Re [23]:

$$\mathrm{Re}_i = \left[\frac{Nu_N}{0.583}\right]^{1/0.471}$$
$$\mathrm{Re}_{eff} = \sqrt{\mathrm{Re}_i^2 + \mathrm{Re}^2} \quad (4e)$$
$$Nu_M = 0.583\mathrm{Re}_{eff}^{0.471}$$

With the Nusselt number known, implementing Eq. (3) – (4) into Eq. (2), we have:

$$r = \frac{Nu{\cdot}k{\cdot}A(T_s - T_{amb})}{DQ_{rad}} \quad (5)$$

The ratio contains the characteristics of both the lamps and duct airflow field; thus, it is expected that the three studies are comparable using the dimensionless parameter r. To find r, it is critical to determine the lamp surface temperature because different operational conditions and lamps result in different surface temperatures. The lamp surface temperature T_s can be calculated using:

$$Q_{total} = Power\ input - UVC\ output = Q_{conv} + Q_{rad}\sqrt{b^2 - 4ac} = \frac{Nu{\cdot}k}{D}A(T_s - T_{amb}) + \varepsilon A\sigma\left[(T_s + 273)^4 - (T_{amb} + 273)^4\right] \quad (6)$$

where Q_{total} is the total heat dissipated by the lamp, which equals the input power minus the fraction of input emitted as UVC and other non-thermal radiation. With Q_{total} (provided by the manufacturer's technical data) and the operating conditions known, the corresponding lamp surface temperature can be calculated. Further, by implementing it back into Eq. (5), the convective heat loss ratio was calculated, as illustrated in Fig. 1.

The lamp surface temperature varies significantly with different lamp characteristics (lamp length, diameter, power input, and UVC output), resulting in lamp output variation, which implies that empirical correlations cannot predict the correct lamp output for other studies. However, the convective heat loss ratio r remains constant among different studies under the same operating conditions (variations from 0.03% to 7.04%). This result is reasonable, as the ratio r is a dimensionless parameter that incorporates the lamp shape and working power. Furthermore, the ratio r is much larger for a lamp operating under forced convection (Fig. 1b and c) than for that under mixed convection (Fig. 1a), which indicates stronger convective heat transfer. This

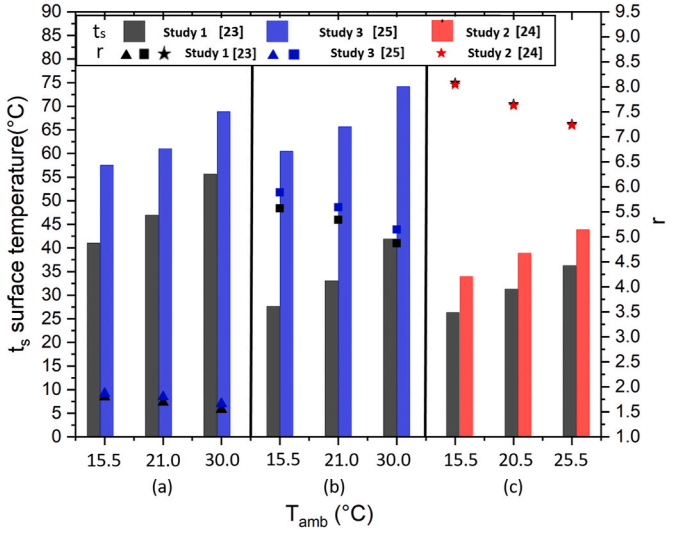

Fig. 1. Predicted lamp surface temperature and convective heat loss ratio r for (a) mixed convection (U = 0.31 m/s) with lamp type 1; (b) forced convection (U = 2.5 m/s) with lamp type 1; (c) forced convection (U = 3 m/s) with lamp type 2.

observation is confirmed by the higher lamp surface temperature in Fig. 1a, which shows that overheating is an issue for mixed convection, whereas the wind-chill effects are dominant for forced convection (Fig. 1b and c). However, uncertainty may arise when applying the r method correlating lamps from different manufacturers, as the r difference in Fig. 1a and b (one lamp from Philips and one lamp from Steril-Aire) is higher than that in Fig. 1c (both lamps are from Philips). Overall, it is promising to bridge the performance of the same type of UV lamps by the ratio r. In other words, for each type of UV lamp, once the convective heat loss ratio r under different operating conditions is experimentally or numerically determined, variations in lamp characteristics (diameter, length, and power) can easily be converted to the new T_s using Eq. (5). Thus, the corresponding performance of each type of lamp can be estimated using the manufacturer's technical data. To examine this hypothesis, the lamp surface temperature and lamp output curve of Studies 2 (type 2) [24] and 3 (type 1) [25] using the r method (r obtained from Study 1 [23]) are computed and plotted below.

The predicted trends in Fig. 2 agree well with the measured irradiance variations in Studies 2 [24] and 3 [25]: the irradiance decreases with increasing ambient temperature in Study 3 [25] for mixed convection (over-heating); the irradiance increases with increasing ambient temperature in Study 3 [25] for forced convection (over-cooling); the irradiance increases and then decreases with increasing ambient temperature in Study 2 [24] for forced convection. However, because of the lack of exact data on lamp output and lamp surface temperature from these two studies, only the trends are compared here, which qualitatively illustrates the applicability of the r method. Further studies are required to measure the lamp surface temperature accurately and examine the r method quantitatively. Finally, it should be noted that the aging and soiling effects of lamps are critical factors that attenuate lamp performance. However, these long-term effects are beyond the scope of most UVGI studies. Thus, in addition to the specifically documented burn-in period in some papers (100 h in Study 1 [23] and EPA studies [29–36]), most results of lamp performance, UV rate constants, and energy consumption were based on the new installations only.

2.1.2. UVC-LED lamp

Despite the extensive use of conventional mercury-type UVC devices, they have disadvantages: the short lifespan and frequent replacement (4000–10000 h), large size light fixture, uncertain lamp surface temperature, a requirement of warm-up time (about 5 min), and mercury as a toxic environmental contaminant [37,38]. Thus, UVC light-emitting diodes (LEDs) are alternative materials to replace conventional mercury-containing UV lamps, UVC-LEDs can produce UV light in different wavelengths compare to the peak irradiation (254 nm) produced by the conventional mercury-based UV lamps. The summary of the limited UV-LED systems eliminating airborne microorganisms in literature is presented in Supplementary Material Table S2. For bacteria, all the data report higher UV rate constants in the UV-LED system than those in the conventional mercury-type UVGI system, whereas for two viruses (bacteriophages MS2 and ΦX174), opposite trends are found. This variation is attributed to the different wavelengths in the two systems. The radiation peaks at 270.8 nm [37,39] and 280 nm [40] for the LEDs compare to the 253.7 nm for the conventional mercury-type UV lamps. For bacteria, DNA destruction is the primary reason for inactivation, and the DNA of most microorganisms has a peak absorption between 260 nm and 270 nm [41]. Thus, one expects that the bacteria show higher UV rate constants within a 271 nm UV-LED system [37,39]. Moreover, 254 nm and 280 nm fall away from the peak UV absorption spectrum. Thus, small differences are observed for these two wavelengths (Supplementary Material Table S2) [41]. As for the bacteriophage, previous research shows that the loss of MS2 viral infectivity is mainly due to RNA damage [42]. The spectral sensitivity of the MS2 RNA shows lower UV absorbance and viral infectivity at 280 nm than at 254 nm [9], which agrees with the reported lower UV rate constants of MS2 and ΦX174 for the UV-LED system.

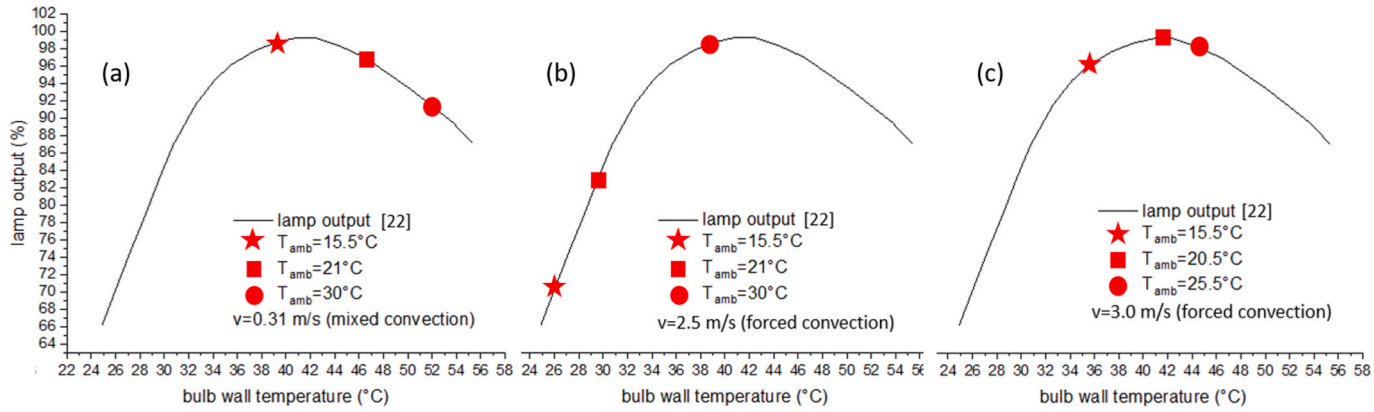

Fig. 2. Predicted lamp surface temperature and lamp output using r method (a) Study 3 [25] mixed convection (b) Study 3 [25] forced convection (c) Study 2 [24] forced convection.

In the future, it is expected that by adjusting the LED peak emitting radiation at 260–270 nm, a higher UV rate constant can be obtained owing to higher UV absorption. At present, UV-LED based in-duct air disinfection systems exist in the prototype stage only, mainly due to limited LED output power. With the development and production of the higher output LEDs, it is expected that UV-LED devices will take a substantial share of the present market, which is occupied by traditional vapor discharge lamps.

2.2. UV rate constants

The UV rate constant k is a species-dependent property of microorganisms that correlates the inactivation efficiency with the UV dose. Several studies have summarized the UV rate constants of different bacteria, viruses, and fungi, for which a comprehensive UV rate constant database was established [10]. However, most of the collected data are water solution-based. In general, the susceptibility of airborne microbes to UV is much greater than that of microbes in suspensions or films on the surface of agar plates. The reasons are as follows: 1) the UV absorptivity of water has an impact; 2) more turbulence and diffusion in air than in water results in more evenly exposed microorganisms; 3) the aerosolization process reduces the microbial survival potential through physical damage; and 4) the oxygenation in air contributes to the increased vulnerability [10]. Consequently, directly applying the UV rate constant from the database underestimates the UVGI system performance in aerosol-based in-duct applications. Thus, to provide insights into the UV rate constants of airborne microorganisms, this paper summarizes the airborne UV rate constants of several human respiratory viruses and surrogates in the literature and tabulates them in Supplementary Material Table S3.

Bacteriophages as surrogates account for most of the investigations due to the low risk and similar size to the real viruses. There is no significant difference between the UV inactivation rate constants of phages and animal viruses. Thus, it is reasonable to use phages as substitutes for animal viruses in inactivation experiments. In Supplementary Material Table S3, most viruses show UV rate constants on the order of 0.1 m^2/J. Among the viruses, RH is found to have a mixed influence on UV sensitivity. Most of them experience lower UV rate constant under higher humidity, while some show a small increase in UV rate constant with increasing RH (i.e., MS2 and Adenovirus). No general explanation has emerged, but some studies interpret the results owing to the formation of a bound water layer that absorbs UV and increases UV light scattering [10]. However, it should be noted that viruses do not appear to respond significantly to relative humidity variations compared to the species differences.

Targeting the COVID-19 mitigation, UVGI has been recommended as an effective method for eliminating airborne SARS-CoV-2 during air recirculation [7]. Thus, the UVGI studies challenged by coronaviruses are summarized in Table 1, providing insights for SARS-CoV-2 applications.

SARS-CoV and SARS-CoV-2 have the same UV dose-response characteristics as they are phylogenetically related, and both belong to the *Sarbecivirus* subgenus [58,59]. In addition, the phylogenetic tree analysis showed that SARS-CoV-2 and SARS-CoV belong to different clades (Clade I, cluster IIa, and IIb) compared with MERS-CoV (Merbecovirus, Clade II) [58,60–62], which elucidates the difference in the UV rate constant between SARS-CoV/SARS-CoV-2 and MERS-CoV. However, it should be noted that most studies were conducted on a liquid-well plate, and their UV rate constants were at least one order of magnitude smaller than those in aerosols, which agrees with the previous finding that the effect of UV absorption is much more significant in water than in air [10]. Therefore, directly applying the UV rate constant extracted from Table 1 will underestimate the UVGI performance (lower UV rate constant of microbes in water than in aerosols). To convert available laboratory data from the liquid phase to the aerosol phase, some studies introduced a species-dependent concept of "UV rate constant ratio of

Table 1
UV rate constants for coronavirus.

Phase	Coronavirus type	Paper	k (m2/J)	D_{90} (J/m2)
Liquid well plate	SARS-CoV-2	[43]	0.0611	37.7
		[44]	0.0025	921.1
		[45]	0.0188	122.5
		[46]	0.0370	62.2
	SARS-CoV	[47]	0.0181	127.3
		[48]	0.0575	40.1
		[49]	0.0008	2878.3
		[50]	0.0002	11599.9
		[51]	0.0111 (no soiling agent) 0.0091 (Mucin) 0.0099 (Sebum)	207.5 (no soiling agent) 253.1 (Mucin) 232.6 (Sebum)
		[52]	0.0093	247.6
	MERS-CoV	[53]	0.0094	244.9
		[51]	0.0104 (no soiling agent) 0.0089 (Mucin) 0.0093 (Sebum)	221.4 (no soiling agent) 258.8 (Mucin) 247.6 (Sebum)
	MHV coronavirus	[54]	0.0266 (MHV 2) 0.0190 (MHV N)	86.7 121.0
		[55]	0.0224	102.8
Aerosol	Human Coronavirus	[56]	0.41 (HCoV-229E) 0.59 (HCoV-OC43)	5.6 (HCoV-229E) 3.9 (HCoV-OC43)
	MHV coronavirus	[57]	0.377	6.1

aerosol and liquid" to correlate the UV rate constant of a group of the same types of viruses in different phases [57,63]. Using this methodology, researchers estimated that the UV rate constant of the coronavirus in air is 1.8–6.0 times higher than that in liquid [63]. However, the estimation was made inter-species between the murine hepatitis virus (MHV) in air and SARS-CoV-2 in liquid, which requires further validation. Thus, this paper deduces the k value of SARS-CoV-2 in air using the UV rate constant ratio calculated only from the MHV coronavirus (in air and liquid). The MHV was chosen as the bridge for estimating the k ratio of SARS-CoV-2 because they belong to the same genus with structural and morphological similarities [64]. Moreover, it has been reported that the MHV can be used as a surrogate for SARS-CoV-2 and other human CoVs because of the similar decay and recovery rates from persistence studies in wastewaters [65,66]. Furthermore, it has been successfully used as a surrogate for SARS-CoV viral aerosols in a chamber for UVGI studies [57]. Therefore, without any known UV rate constants of SARS-CoV or SARS-CoV-2, the MHV can be used to provide the k ratio of air/water and estimate the CoV family's UV rate constants in the aerosol phase. Accordingly, we have the average k value of the MHV in liquid and air as 0.0227 m^2/J and 0.377 m^2/J, respectively, which gives a k ratio of 16.61. Upon implementing the obtained k ratio, the UV rate constants of coronaviruses in air were estimated to be 0.4958 m^2/J (SARS-CoV-2) and 0.3942 m^2/J (SARS-CoV). The estimation is close to the average k value (0.459 m^2/J) for coronaviruses in air (MHV coronavirus, HCoV-229E, and HCoV-OC43) (Table 1), which elucidates the applicability of the estimation method.

3. In-duct UVGI system applications

3.1. In-duct UVGI system designs in literature and disinfection performance

This paper summarizes most of the in-duct UVGI system designs and the reported UV doses in the literature (Table 2). Furthermore, for COVID-19 mitigation, the estimated CoV UV rate constants (Section 2.2) were incorporated with the case-specific UV dose to evaluate the coronavirus disinfection by current in-duct UVGI system designs.

Twenty-four different designs are listed in Table 2. Among them, the U.S. Environmental Protection Agency (EPA) conducts a series of real-life in-duct UVGI investigations with various lamp arrangements, which are essential guidelines for in-duct UVGI system designs. The reported UV dose range covers from 2.47 to 423.42 J/m^2, which corresponds to disinfection efficacies of 70.61%–100.00% and 62.23%–100.00% for SARS-CoV-2 and SARS-CoV, respectively. For a proper UVGI system with the capability to inactivate 99% SARS-CoV-2 in air during the COVID-19 pandemic, in-duct UVGI systems #1, #4, #5, and #7 may be considered. For instance, a system using six lamps with aluminum foil-lined ducts following Design #4 [32] provides a UV dose of 198.26 J/m^2. Most other systems provide sufficient UV doses for 90% SARS-CoV-2 inactivation, except for Designs #11, #13, and #14, in which because of the high airflow velocities (6, 5, and 6.5 m/s), the exposure time was shortened and the lamp output was decreased (wind-chill impact). Further, the HVAC operating conditions are taken into consideration, with reports that 30 °C and 1 m/s lead to the highest UV doses (133.74 and 110.21 J/m^2 for four lamps perpendicular or parallel to the airflow), while 10 °C and 3 m/s result in 44.58 and 36.74 J/m^2 for perpendicular or parallel directions owing to the over-cooling of UV lamps [67]. Overall, an appropriate in-duct UVGI system design should provide an average UV dose of at least 4.64 J/m^2 and 5.84 J/m^2 for 90% SARS-CoV-2 and SARS-CoV inactivation. Thus, more powerful lamps or a slower airflow are required to increase the UV dose in the ductwork.

3.2. In-duct UVGI system modeling

3.2.1. Optimization of the in-duct UVGI system using CFD simulation

Computational fluid dynamics (CFD) simulation of the in-duct UVGI system has gained popularity in recent years owing to its ability to simulate complex in-duct airflows, providing a microscopic view of the fluid/thermal physical phenomenon and detailed information on the physics quantity field [70]. Radiative and airborne microorganism transport are the two major concerns in the in-duct UVGI air sterilization system simulation.

In general, the radiative transfer equation (RTE), which considers varying isothermal conditions, such as absorption, reflection, and refraction, is established to compute the irradiance field of the duct. Commonly used models include the P1 model [71], surface-to-surface model (S2S) [72], and the discrete ordinates (DO) model [71,73–76]. As for airborne microorganism transport, CFD simulation with the discrete phase model (DPM), which solves the particle trajectory based on Newton's second law and accounts for gravity, drag force, and momentum coupling between the particle and the fluid, is commonly used [77]. By solving the DPM equations along with the velocity vector of air, the motions of airborne organisms can be tracked, and the spatial and temporal concentrations (number of particles in each computational cell at any time t) can be determined. By further combining the UV irradiance field with the bioaerosol trajectories, the cumulative UV dose of individual particles and the average UV dose (standard deviation) of the system can be computed.

The average UV doses (standard deviations) and dose distributions are the critical indices that CFD simulations provide for UVGI system evaluation. CFD has been successfully applied in the literature to provide an accurate overall average UV dose for a system. For instance, the EPA 600/R-06/050 test experimentally rated the performance of a single-lamp UV system of 2.47 J/m^2 (Design #2 in Table 2) from *B. atrophaeus*. However, CFD simulation shows that the average UV dose should be 10.97 J/m^2, a more accurate dose value that gives closer disinfection efficacy for MS2 with the experimental results [78]. In the same manner, the average UV dose for EPA 600/R-06/051 (Table 2) was corrected from 2.95 to 18 [10], 18.3 [79] and 18.45 J/m^2 [78] using CFD simulations. The UV dose differences in the three simulation results are attributed to the particle trajectories within the system, the 25% or 15% diffusive wall reflectivity used, and the different particle characteristics. In addition, the impact of varying particle sizes (ranging from 1 $\times 10^{-6}$ to 1 $\times 10^{-4}$ m and 3 $\times 10^{-7}$ to 3 $\times 10^{-6}$ m) on the UV dose was observed by the 0.25% reduced sterilization performance, which was reasonable as the particle's surface area and the UV dose slightly reduced with particle diameter [80]. In addition to estimating the average UV dose of a UVGI system, the CFD simulation with the DPM can reveal the cumulative UV dose distribution with respect to particle counts and the standard deviation of the system average UV dose, which is particularly important from the perspective of inactivating an individual microorganism. For instance, a study shows that an arrangement of four vertical lamps has an average UV dose and standard deviation of 18.3 and 4.17 J/m^2 [79]. In reality, the overdosed UV irradiance on one particle will not transfer to and average with other underexposed particles, resulting in the wasted energy input for the overdosed bioaerosols and insufficient characterization of a system with the average UV dose. Furthermore, research shows that a system with the highest average UV dose (regardless of the standard deviation) performs better on a strongly resistant microorganism. In contrast, for a weak microorganism, a system with a more evenly distributed UV dose (lower standard deviation) is needed, even with a lower average UV dose [81].

With the provided accurate average UV dose and standard deviation along with its advantages in terms of cost and time compared to experimental investigations, the CFD analysis was applied to conduct the parametric studies and UVGI system design optimizations. For instance, the three-lamp array optimization was conducted in six arrangements (see Supplementary Material Fig. S1), which resulted in

Table 2
In-duct UVGI system designs in literature and the estimated coronavirus inactivation efficiencies.

Design details							Reported inactivation efficiency in literature	Estimated inactivation efficiency (log reduction) in this study	
Design No.	Duct size W × H × L (m × m × m)	Lamp arrangement (lamp numbers, direction)	Power (W)	UV dose (J/m^2)	Airflow (m/s)	Environmental conditions		SARS-CoV-2	SARS-CoV
#1 (EPA 600/R-06/049) [29]	0.61 × 0.61 × 4.6[a]	12[b], reflective duct material	720	76.51	2.5	23.2–24.1 °C	MS2 98%	~100%[d] (16.47)	~100% (13.10)
#2 (EPA 600/R-06/050) [30]		1, perpendicular	58	2.47		22.7–22.9 °C	39%	70.61% (0.53)	62.23% (0.42)
#3 (EPA 600/R-06/051) [31]		4, perpendicular	100	2.95		23–23.2 °C	46%	76.84% (0.64)	68.74% (0.51)
#4 (EPA 600/R-06/052) [32]		6, perpendicular[c], reflective	420	198.26		25.3–25.8 °C	99%	~100% (42.69)	~100% (33.94)
#5 (EPA 600/R-06/053) [33]		5, parallel	1100	164.39		24.4–24.8 °C	99%	~100% (35.40)	~100% (28.14)
#6 (EPA 600/R-06/054) [34]		4, perpendicular	240	5.82		23–23.2 °C	75%	94.42% (1.25)	89.92% (0.99)
#7 (EPA 600/R-06/084) [35]	0.3 × 0.3 × 4.6[a]	6, parallel, reflective	750	423.42	1.56	21.2–24.1 °C	100%	~100% (91.17)	~100% (72.49)
#8 (EPA 600/R-06/085) [36]	0.61 × 0.61 × 4.6[a]	12, pulsed, perpendicular	7020	4.47	2.72	23.6–25.2 °C	59%	89.10% (0.96)	82.83% (0.77)
#9 [19]	0.2 × 0.2 × 1.4	1, perpendicular	9	7.35	3	23 °C, 55%	SM (99.925%); PA (99.909%); EC (98.168%); SE1 (93.607%); SE2 (92.935%)	97.39% (1.58)	94.48% (1.26)
#10 [19]				4.90	4.5		–	91.19% (1.06)	85.51% (0.84)
#11 [19]				3.68	6		–	83.83% (0.79)	76.51% (0.63)
#12 [24]	0.2 × 0.2 × 1.4	1, perpendicular	9	6.52	3	20 °C, 50%	SE2 (81.73%); PA (99.75%); EC (95.92%)	96.05% (1.40)	92.35% (1.12)
#13 [24]				3.91	5		–	85.62% (0.84)	78.61% (0.67)
#14 [24]				3.01	6.5		–	77.52% (0.65)	69.47% (0.52)
#15 [67]	0.61 × 0.61 × 2.74	4, perpendicular	240	66.87	2	20 °C	–	~100% (14.40)	~100% (11.45)
#16 [67]				44.58	3	10 °C	–	~100% (9.60)	~100% (7.63)
#17 [67]				133.74	1	30 °C	–	~100% (28.80)	~100% (22.90)
#18 [67]		4, parallel		55.11	2	20 °C	–	~100% (11.87)	~100% (9.43)
#19 [67]				36.74	3	10 °C	–	~100% (7.91)	~100% (6.29)
#20 [67]				110.21	1	30 °C	–	~100% (23.73)	~100% (18.87)
#21 [68]	0.64 × 0.64 × 2.44	4, parallel	240	6.30	0.93	22.7 °C; 31%	MS2 (99.21%); BB (99.94%); FH (43.77%); CD (96.84%)	95.60% (1.36)	91.65% (1.08)
#22 [25]	0.61 × 0.61 × 3.54	1, perpendicular	145	13.41	1.27	24 °C, 50%	SM (99%); SE (81%);	99.87% (2.89)	99.49% (2.30)
#23 [25]		3, perpendicular	435	31.97			BS (50.5%); AV (10.5%); PC (0.5%); CS (9.5%)	~100% (6.88)	~100% (5.47)
#24 [25]		6, perpendicular	870	75.09					

(*continued on next page*)

Table 2 (*continued*)

Design details							Reported inactivation efficiency in literature	Estimated inactivation efficiency (log reduction) in this study	
Design No.	Duct size W × H × L (m × m × m)	Lamp arrangement (lamp numbers, direction)	Power (W)	UV dose (J/m^2)	Airflow (m/s)	Environmental conditions		SARS-CoV-2	SARS-CoV
							BS (85%); AV (74.5%); PC (13.5%); CS (16%)	~100% (16.17)	~100% (12.86)

SM: S.marcescens; PA: P.alcaligenes; SE1: S.enterrica; SE2: S.epidermidis; EC: E.coli; BB: B.broncbiseptica; FH: feline herpesvirus-1; CD: canine distemper virus; BS: Bacillus subtilis; AV: Aspergillus versicolor; PC: Penicillum chrysogenum; CS: Cladosporium sphaerospermum.

[a] Duct length estimated by ASHRAE standard 52.2 [69].

[b] Lamp arrangement details in Ref. [29].

[c] Lamp arrangement details in Ref. [32].

[d] For inactivation efficiency greater than 99.995%, we present "~100%".

average UV doses (standard deviations) of 28.33 (10.06), 28.21 (5.39), 27.91 (16.32), 30.18 (12.60), 26.45 (5.37) and 31.05 J/m^2 (5.45 J/m^2), respectively [81]. From a UVGI system design perspective, a higher average UV dose and a single sharp peak (lower UV dose standard deviation) with all particles receiving the required UV dose is expected [78,79,81]. Thus, the lamp array with all three lamps located at the center of the duct and distributed across its height provides the best performance (average UV dose of 31.05 J/m^2 and standard deviation of 5.45 J/m^2). In addition to the lamp array arrangements, other design parameters, such as the number of lamps, lamp orientations, and duct materials, are numerically evaluated, and the corresponding design suggestions are presented in Table 3.

3.2.2. Energy simulation of the in-duct UVGI system

In the literature, the inactivation effectiveness of UVGI systems has been extensively studied, while energy and cost discussions are rarely reported. The air temperature, air velocity, relative humidity, device geometry, and lamp characteristics (power, geometry, and wavelength) are critical for characterizing the UV inactivation efficiency and energy consumption. Previous research has addressed the energy simulation and life-cost analysis of an in-duct UVGI system from the perspective of lamp output, meteorological climate (cold, hot, and warm climate zones), and installation locations (downstream and upstream of the cooling coil for the conditioned supply air and unconditioned mixed air) [17,18,83]. The results show that installing the lamps downstream from the cooling coil (supply air) led to a stable air temperature and stable energy consumption for all three climate zones. However, the conditioned air after the cooling coil also results in a lower lamp surface temperature and lower lamp output, leading to higher costs than the installation upstream of the cooling coil. Meanwhile, owing to the mixed outdoor air and recirculating air, the energy consumption of the UVGI system located upstream of the cooling coil is highly dependent on the meteorological climate. For instance, New York requires much higher lamp input power and energy consumption during the winter because of the low outdoor temperature and low lamp output. In contrast, the mild climate in Los Angeles leads to low energy consumption due to the narrow range of lamp output, which allows the operational inactivation efficiency to be very close to its design value [83].

Despite the insights of meteorological climate and installation locations on the UVGI system energy consumption, the previous work neglects humidity. It adopted 0.35 m^2/J as the *S. aureus* UV rate constant, obtained under saturated environmental conditions (T = 22.5 °C and RH = 95%) [84]. Thus, significant deviations are expected owing to the incomparable humidity conditions. In this paper, the effect of humidity on the UV rate constant is incorporated to illustrate the energy consumption for all three operational factors (air temperature, velocity, and humidity) for the UVGI system installation downstream from the cooling coil (supply air). For this purpose, an empirical correlation between the humidity ratio and UV rate constant for airborne *S. aureus* was extracted in the literature [85]:

$$UVsusceptibility = 0.0609 \times humidityratio^{-0.407} \left(R^2 = 0.9919\right)$$

$$humidityratio\left(g/kg\right) = \frac{6109.4 \times R_{da} \times RH\% \times \exp\left(\frac{17.625 T_{amb}}{T_{amb}+243.04}\right)}{R_v\left(P_{da} + (RH\% - 1) \times 6.1094 \times \exp\left(\frac{17.625 T_{amb}}{T_{amb}+243.04}\right)\right)} \tag{7}$$

where R_{da} and R_v are the specific gas constants of dry air and water vapor, and P_{da} is the pressure of dry air (assuming 101.325 kPa as the international standard atmosphere at the standard sea-level, 15 °C). Eq. (7) is then applied in Sharp's study [84] to obtain the UV rate constants under different humidity conditions. As the reference UV rate constants are known (0.35 m^2/J compared to the 0.01976 m^2/J computed from Eq. (7) under the same environmental conditions, T = 22.5 °C and RH = 95%), the scaling factor is computed (17.71), and the UV rate constants under different average monthly environmental conditions can be scaled accordingly:

$$UVsusceptibility = 1.079 \times \left[\frac{6109.4 \times R_{da} \times RH\% \times \exp\left(\frac{17.625 T_{amb}}{T_{amb}+243.04}\right)}{R_v\left(P_{da} + (RH\% - 1) \times 6.1094 \times \exp\left(\frac{17.625 T_{amb}}{T_{amb}+243.04}\right)\right)}\right]^{-0.407} \tag{8}$$

For the expected 85% inactivation efficiency, the required lamp power input is obtained by scaling the given lamp power and emitted fluence rate relationship from the original paper [83] as:

$$\text{Input power} = \frac{\text{Fluence rate}}{9.05} = \frac{\text{UV dose}}{\text{Lamp output} \times \text{exposure time} \times 9.05} = \frac{-\ln(0.15)}{k \times \text{Lamp output} \times \text{exposure time} \times 9.05} \tag{9}$$

By implementing the UV rate constant (Eq. (8)), lamp output (type 1 cross-flow [23]), and exposure time ([83]) into Eq. (9), the lamp power input P (W) can be written as:

$$P = \frac{0.249U}{\frac{6109.4R_{da}RH\%\exp\left(\frac{17.625T_{amb}}{T_{amb}+243.04}\right)}{R_v\left(P_{da}+(RH\%-1)\times 6.1094\ \exp\left(\frac{17.625T_{amb}}{T_{amb}+243.04}\right)\right)}-0.407}\left(5.79+5.56T_{amb}-20.3U-0.0701T_{amb}^2+4.01U^2\right) \quad (10)$$

By further multiplying the working hours, the lamp energy consumption can be estimated as a function of the three operational parameters (T, U, and RH). Thus, the variance-based global sensitivity analysis (Sobol method) is used to evaluate the influence of each parameter contributing to the variations in P. Next, the total-order index (ST), which measures both the direct and indirect contributions of each parameter to the final output variance and its confidence level, are computed and tabulated in Table 4. Furthermore, to better illustrate the direct effect of individual parameters on the overall energy consumption, the monthly energy variation ratios (monthly energy consumption divided by the worst month's energy consumption) were calculated while keeping the other two parameters constant (yearly average values). The results are shown in Fig. 3.

Owing to small variations in the temperature at the air supply locations, the temperature has only 0.0298–0.0615 total-order indices among all three climates, which indicates the weak influence of varying temperature on the lamp power input requirement. Over a single year, summer was found to have a lower energy consumption than winter (Fig. 3), which is attributed to the higher air temperature and thus higher lamp output. Air velocity is the dominant parameter in defining the power input, and in contrast to the trend of air temperature, summer reports much higher energy consumption than winter among all three cities. This finding is reasonable as the air velocity affects both the lamp output ratio and the exposure time of the microorganisms. In other words, owing to the large conditioning capacity required in the summer, the increased air velocity decreases the lamp output and shortens the exposure time, thus demanding higher lamp power. Humidity imposes a varying influence from negligible to moderate across different climate zones. For a hot and humid climate (Houston), humidity is high and almost constant; thus, a negligible seasonal difference is observed. In contrast, in a mildly warm climate (Los Angeles), 15% humidity variation has a significant impact on the lamp input power compared to the other two locations. Analogous to air velocity, the higher humidity ratio in summer results in a lower UV rate constant, and thus higher energy consumption. The confidence levels were very small (Table 4), indicating sufficient data samples for a sensitivity analysis. Because the relative humidity is identified as a non-negligible environmental factor, previous works that neglect humidity gave incorrect estimations. Thus, in this paper, the humidity-amended UV rate constants are incorporated, and the newly predicted monthly energy consumption and variation ratios are presented in Supplementary Material Table S4 and Fig. 4, respectively.

The total energy consumption of the three cities was similar because of the similar supply air condition requirements. Analogous to Fig. 3, July has the highest energy consumption throughout the year. This is attributed to the higher moisture that lowers the UV rate constant, even though a higher lamp output is reached under the optimal air

Table 3
In-duct UVGI system design suggestions from the literature data.

Paper	Duct size W × H × L (m × m × m)	Lamp arrangement (lamp numbers, direction)	Average UV dose (standard deviation) (J/m2)	Conclusions
[23]	0.61 × 0.61 × 2.74	4, perpendicular	53.19–6479.66	1. Without considering the thermal effect on the lamp output, placing UV lamps in a crossflow gives higher UV irradiance.
		4, parallel	121.30–3732.26	2. Considering the wind chill effects, arranging lamps in parallel flow provides a higher average irradiance for a system with lower temperature and higher airflow.
[81]	0.61 × 0.61 × 1.83	1, perpendicular, 6 locations in the duct	7.87–9.51	1. Placing the UV lamp at the duct center (height and length) provides the best average UV dose. 2. Lamp locates at the beginning of the duct performs better than locates at the end of the duct.
		1, center of the duct, perpendicular	10.97 (4.39)	3. Lamp locates parallel to the airflow provides higher average UV dose.
		1, center of the duct, parallel	17.36 (16.27)	4. Higher standard deviation of the UV dose is observed for parallel scenario, indicating some particles receive a considerably lower UV dose than the average of the system.
		3 lamps, perpendicular (arrangements see Supplementary Material Fig. S1)	28.33 (10.06) 28.21 (5.39) 27.91 (16.32) 30.18 (12.60) 26.45 (5.37) 31.05 (5.45)	5. The best performance is achieved by locating all three lamps at the center of the duct and distributed across the height of the duct. 6. The more even the UV dose distribution is, the more efficient the system is. 7. Increasing the lamp numbers increases the UV dose distribution uniformity and indicates better energy usage.
[79]	0.61 × 0.61 × 1.83	4, perpendicular 4, 30° perpendicular 4, 60° perpendicular 4, parallel	18.3 (4.17) 18.49 (4.60) 19.12 (6.75) 18.39 (7.89)	1. UV dose distribution non-uniformity (UV dose standard deviation) increases when changing the lamp array configuration from vertical to horizontal.
[82]	0.02 × 0.02 × 0.12	48 LEDs (at the floor and ceiling of the duct) 72 LEDs (at the floor and ceiling of the duct)	–	1. The use of highly reflective surfaces significantly increases microbial inactivation and minimizes the impact of LED positions on inactivation levels. 2. Four wall reflection results in higher inactivation rates than solely side-side or top-bottom surface reflection. 3. The number of LEDs controls the maximum inactivation level when there are more than three reflection walls.

Table 4
Sensitivity analysis of the lamp power input with respect to the influence of air temperature, air velocity and relative humidity.

City	T (°C)	U (m/s)	RH	Total-order index (confidence level)		
				T	U	RH
New York	9.68–10.45	1.50–1.89	0.57–0.67	0.0599 (6.16×10^{-4})	0.9016 (7.51×10^{-3})	0.0398 (3.99×10^{-4})
Houston	10.06–10.62	1.55–1.91	0.73–0.77	0.0382 (4.21×10^{-4})	0.9566 (7.54×10^{-3})	0.0058 (5.82×10^{-5})
Los Angeles	10.17–10.46	1.71–1.90	0.56–0.71	0.0291 (3.31×10^{-4})	0.6614 (5.68×10^{-3})	0.3101 (3.36×10^{-3})

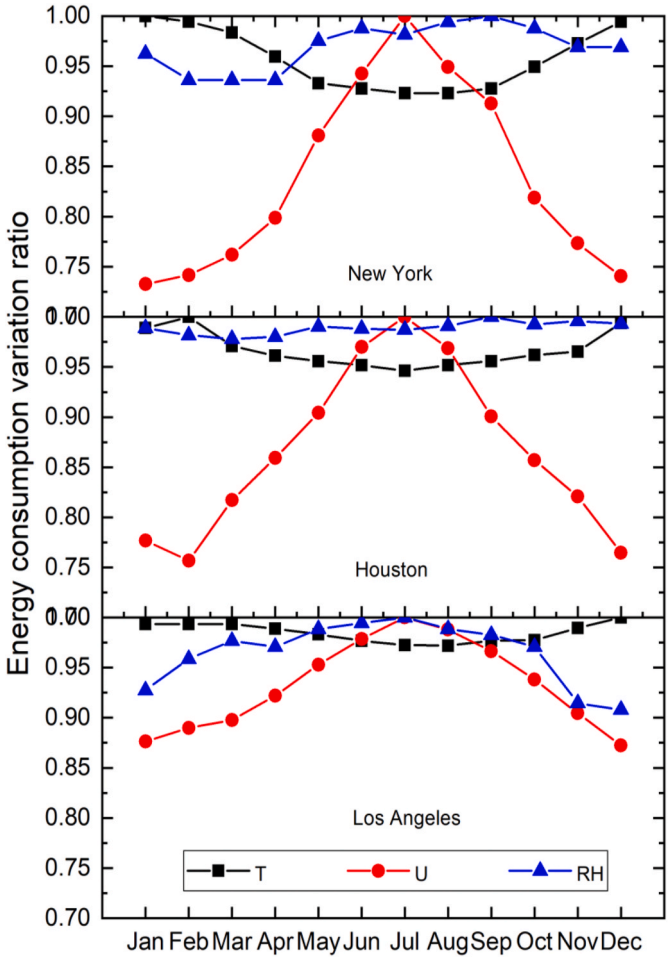

Fig. 3. Direct effect of air temperature, air velocity and relative humidity on the monthly energy consumption variation ratios across three climate zones.

temperature and velocity. As shown in Supplementary Material Table S4, the humidity-amended energy consumption decreases because the reported UV rate constant for *S. aureus* in a saturated environment (RH = 95%) is lower than that in the real conditioned supply air. Comparing the monthly energy consumption variation ratio, the effects of humidity vary from climate to climate, and the trend agrees with the sensitivity analysis. New York, Houston, and Los Angeles show weak, negligible, and moderate influences from the humidity-amended UV rate constants. Particularly during the winter season, the humidity is relatively low with a high UV rate constant, which compensates for the low lamp output and has the minimum energy consumption.

Overall, air velocity was the dominant factor affecting the UVGI system energy consumption in terms of lamp output and exposure time. Relative humidity influences the UV rate constant; thus, it plays a significant role in determining UVGI inactivation and energy consumption performance. Meanwhile, the low-pressure mercury lamps used in previous studies may lead to high replacement capital. Thus, further studies are required to employ UV-LEDs and explore the effect of humidity on the energy consumption of the UVGI system.

3.3. Inactivation performance and energy consumption predictions of in-duct UVGI systems for mitigating COVID-19 transmission

To evaluate the current in-duct UVGI system design strategies (from EPA studies) on COVID-19 mitigation, this review incorporates the lamp output characteristics and SARS-CoV-2 UV rate constants to calculate each design's inactivation efficiency and minimal lamp requirements to maintain 99% inactivation efficiency. The seasonal climates of interest are defined as summer and winter, with each season lasting six months. The full air recirculation scenario was considered in this review to evaluate the worst virus transmission cases. Therefore, the environmental conditions in an HVAC system are defined to be the same as those in an indoor environment. That is to say, maintaining the indoor temperature in the range of 23–26 °C (below 60% RH) and 20–23.5 °C (20%–30% RH) for the cities in North America during the summer and

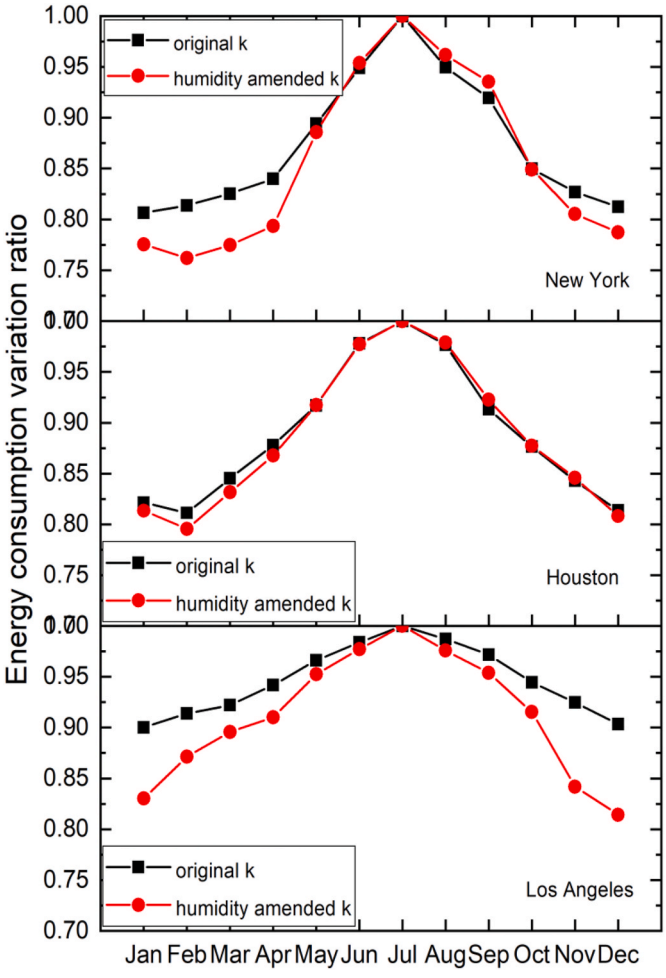

Fig. 4. Comparison of monthly energy consumption variation ratios between the original and humidity amended UV rate constant.

winter seasons, respectively [86,87]. Thus, in this review, the temperature and RH were set as 24.5 °C (60% RH) and 21.7 °C (25% RH) for summer and winter, respectively. With the environmental conditions known, the SARS-CoV-2 UV rate constant correlation is introduced as:

$$k_{SARS-CoV-2} = C_1 \times C_2 \times humidity\,ratio^{C_3}$$
$$= 0.499 \times 3.189 \times \left[\frac{6109.4 \times R_{da} \times RH\% \times \exp\left(\frac{17.625T_{amb}}{T_{amb}+243.04}\right)}{R_v\left(P_{da}+(RH\%-1)\times 6.1094 \times \exp\left(\frac{17.625T_{amb}}{T_{amb}+243.04}\right)\right)}\right]^{-0.554} \quad (11)$$

where $C_2 water\,concentration^{C_3}$ is the UV rate constant and humidity correlation obtained from MS2 [88] due to the lack of humidity dependency of the airborne SARS-CoV-2 UV rate constant, and C_1 is the scaling factor to correlate the different reference k values (T = 22 °C and RH = 50%) between SARS-CoV-2 and MS2. Thus, the estimated UV susceptibilities of SARS-CoV-2 during the summer and winter seasons were 0.4124 m^2/J and 0.7328 m^2/J. The variations compared to the reference k value are due to temperature and humidity effects. Upon implementing the obtained UV rate constants in the reported UV dose for each design, the expected SARS-CoV-2 inactivation efficiencies were computed (Table 5). It has been shown that some designs impose significant waste of UV dose (energy), while others provide insufficient UV dose for 99% SARS-CoV-2 inactivation. Thus, assuming a linear proportional relationship between the number of lamps and the contribution to the overall UV dose in the system, suggestions for sufficient UV lamps in each design to provide the required UV dose are introduced and are tabulated in Table 5. Furthermore, recalling that the lamp output differs for the average summer and winter seasons with the reported design environmental conditions, the lamp surface temperature is computed by rearranging Eqs. (2)–(6) as follows:

For cylinder lamp forced convection :

$$Q_{total} = \left[0.3 + \frac{0.62\mathrm{Re}^{0.5}\mathrm{Pr}^{1/3}}{0.4/\mathrm{Pr}\left(0.4/\mathrm{Pr}\right)(0.4/\mathrm{Pr})^{2/3}\right)^{1/4}}\left[1+\left(\frac{\mathrm{Re}}{282000}\right)^{5/8}\right]^{4/5}\right] k\pi L_{lamp}\left(T_s - T_{amb}\right) \quad (12a)$$
$$+\varepsilon\sigma\pi D_{lamp}L_{lamp}\left[(T_s+273)^4 - (T_{amb}+273)^4\right]$$

Table 5
Design and energy consumption predictions of in-duct UVGI systems in literature for 99% SARS-CoV-2 inactivation (required UV dose: 11.17 J/m^2 for summer and 6.29 J/m^2 for winter).

Original design (from EPA reports)				New design suggestions					
Design details		UV dose (J/m^2)	Inactivation efficiency (log reduction)	Design	UV dose[b] (J/m^2)	Inactivation efficiency (log reduction)	Energy consumption (kW h)		
							Summer	Winter	Year
#1 (EPA 600/R-06/049)[a] [29]	12 lamps (each 60W), reflective duct material	76.51	~100%[c] (13.82) (summer) ~100% (24.19) (winter)	2 lamps	12.75	99.50% (2.30) (summer) 99.99% (4.03) (winter)	525.6	525.6	**1051.2**
#2 (EPA 600/R-06/050) [30]	1 lamp (58W), perpendicular	2.47	65.25% (0.45) (summer) 76.38% (0.78) (winter)	5 lamps (summer) 3 lamps (winter)	12.14 (summer) 7.49 (winter)	99.36% (2.19) (summer) 99.57% (2.37) (winter)	1270.2	762.12	**2032.32**
#3 (EPA 600/R-06/051) [31]	4 lamps (each 25W), perpendicular	2.95	71.70% (0.53) (summer) 82.16% (0.93) (winter)	15 lamps (summer) 9 lamps (winter)	11.30 (summer) 6.48 (winter)	99.09% (2.04) (summer) 99.11% (2.05) (winter)	1462.5	985.5	**2448**
#4 (EPA 600/R-06/052) [32]	6 lamps (each 70W), perpendicular, reflective	198.26	~100% (35.80) (summer) ~100% (62.69) (winter)	1 lamp	33.70 (summer) 34.71 (winter)	~100% (6.09) (summer) ~100% (10.98) (winter)	306.6	306.6	**613.2**
#5 (EPA 600/R-06/053)[a] [33]	5 lamps (each 220W), parallel	164.39	~100% (29.69) (summer) ~100% (51.98) (winter)	1 lamp	32.88	~100% (5.94) (summer) ~100% (10.40) (winter)	963.6	963.6	**1927.2**
#6 (EPA 600/R-06/054) [34]	4 lamps (each 60W), perpendicular	5.82	91.71% (1.05) (summer) 96.66% (1.84) (winter)	8 lamps (summer) 5 lamps (winter)	11.48 (summer) 7.38 (winter)	99.15% (2.07) (summer) 99.54% (2.33) (winter)	2102.4	1314	**3416.4**
#7 (EPA 600/R-06/084)[a] [35]	6 lamps (each 125W), parallel, reflective	423.42	~100% (76.46) (summer) ~100% (133.89) (winter)	1 lamp	70.57	~100% (12.74) (summer) ~100% (22.31) (winter)	547.5	547.5	**1095**
#8 (EPA 600/R-06/085)[a] [36]	12 pulsed lamps (each 585W), perpendicular	4.47	85.23% (0.81) (summer) 92.66% (1.41) (winter)	30 lamps (summer) 17 lamps (winter)	11.18 (summer) 6.33 (winter)	99.01% (2.00) (summer) 99.00% (2.00) (winter)	76,869	43559.1	**120428.1**

[a] The UV dose for 99% inactivation is not corrected by the lamp output for summer and winter weather due to the lack of a heat transfer model for other lamp airflow facing scenarios.
[b] Summer and winter UV doses are different due to the consideration of different lamp output for summer and winter HVAC operating conditions (050, 051, 054, 085: cylinder lamp forced convection).
[c] For inactivation efficiency greater than 99.995%, we present "~100%".

$$For\ twin-tubes\ lamp\ forced\ convection:\quad Q_{total}=\left[0.27\mathrm{Pr}^{0.37}\mathrm{Re}^{0.6}\right]k\pi L_{lamp}(T_s-T_{amb})+\varepsilon\sigma\pi D_{lamp}L_{lamp}\left[(T_s+273)^4-(T_{amb}+273)^4\right] \tag{12b}$$

Solving Eqs. (12a) and (12b) iteratively to calculate the case-specific average lamp surface temperature, the lamp output is then extracted using the manufacturer's datasheet (assuming all the lamps follow the lamp performance curve provided by Philips [22]) as follows:

$$UVC output(\%)=-0.003T_s^3+0.1955T_s^2-0.7163T_s+9.7343\ \ For\ T_s<42.5^{\circ}C$$
$$UVC output(\%)=-1.1784T_s+151.86\ \ For\ T_s>42.5^{\circ}C \tag{13}$$

Finally, the UV doses of the suggested designs are scaled from the original design by considering the operating conditions:

$$D(T_{amb},U,RH)=\left[D_{design}\frac{Lamp\ number}{Lamp\ number_{design}}\right]\times \left[\frac{UVC\ output(T_{amb},U,lamp\ shape,lamp\ power)}{UVC\ output_{design}}\right]\left[\frac{k(T_{amb},RH)}{k_{design}}\right]\left[\frac{U_{design}}{U}\right] \tag{14}$$

A schematic of the UV dose calculation in a ventilation duct is shown in Fig. 5. The inactivation efficiencies and energy consumptions for the design suggestions are listed in Table 5. Significant differences were predicted for energy consumption for different UVGI system designs. Designs #1, #4, and #7 are the most energy-efficient designs from the perspective of energy saving, consuming 1051.2, 613.2, and 1095 kWh per year, respectively, for a minimum of 99% SARS-CoV-2 inactivation. One primary reason for this is the reflective materials used in the UVGI system designs. Among the three designs, Designs #4 and #7 are particularly efficient. They provide a much higher UV dose than the system requires, compared to the mere 99% inactivation efficiency in Design #1, making them more reliable for disinfecting other microorganisms with higher UV resistance. Designs #2 and #5 report moderate energy consumption as they use less reflective wall materials. Furthermore, Design #5 mounts five UV lamps compactly on a parabolic reflector, in which some UV irradiance can be wasted on the reflectors. Designs #3 and #6 consume much more energy because none of them applied reflective wall materials or mirror-like duct walls, whereas Design #8 consumes significant energy because of the pulsed UV lights used, and it is beyond the scope of this comparison. Furthermore, energy savings are achieved by considering the effects of operational factors on the lamp output. Design #3 originally requires 16 lamps to provide a UV dose of 11.8 J/m^2 for 99.26% inactivation during the summer. However, due to the higher lamp output in the summer season (24.5 °C) than that in the original study's experimental condition (23.1 °C), 15 lamps are found to provide sufficient UV dose (11.3 J/m^2) for 99.09% inactivation, which saves 109.5 kWh of energy for the summer season. Finally, it should be noted that the energy consumption predictions in this paper suffer from the linear relationship assumption between the lamp power input and the contributed UV dose in the duct, which neglects the effects of humidity on the radiation transport. Further radiation transport simulation studies are needed to correlate the lamp power input and UV dose in the duct accurately.

4. Conclusions

This paper summarizes four key aspects of designing an in-duct UVGI system: germicidal source output, UV rate constant, system inactivation efficiency, and system energy consumption. The critical technical parameters defining the above aspects are air temperature, air velocity, and relative humidity. The complex interactions between the design elements and operational parameters were elucidated and discussed throughout this review. The conclusions are summarized below.

- The lamp working mechanisms, lamp outputs, and corresponding UV rate constants differ significantly between conventional mercury-based UV lamps and UV-LEDs. For low-pressure mercury UV lamps, air velocity and air temperature critically affect the lamp output owing to the wind-chill effect. This paper introduces a dimensionless parameter r for generally correlating lamp characteristics and wind-chill impact on the heat transfer model base and

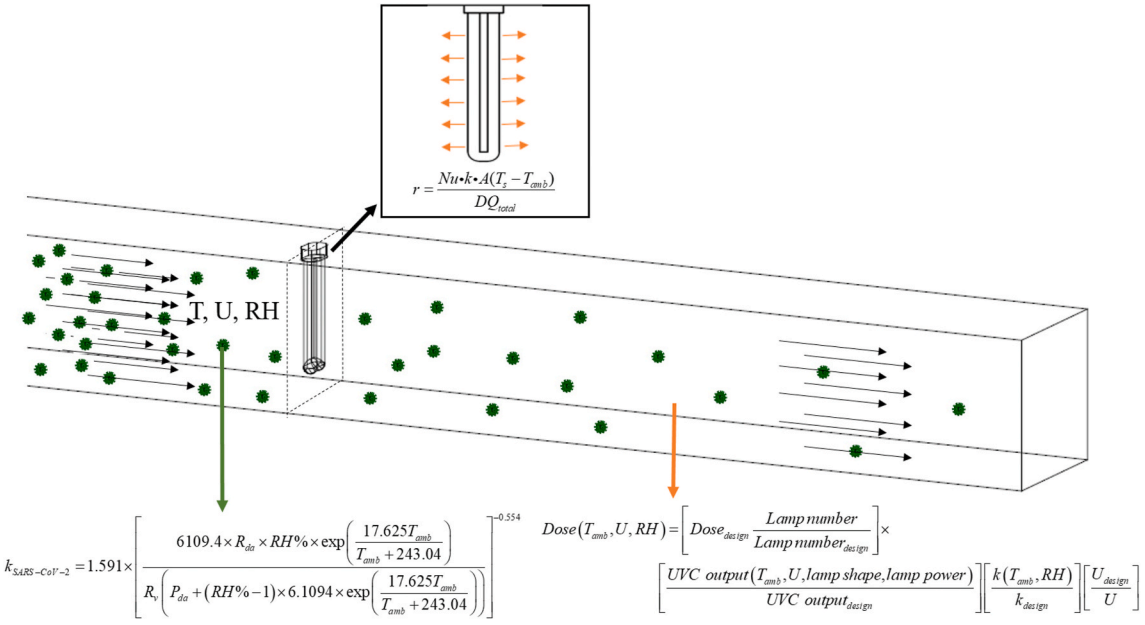

Fig. 5. Schematic diagram of the UV dose calculation in ventilation ducts.

empirical lamp output correlations in the literature. For UV-LEDs, limited conclusions have been drawn owing to the early stage of the investigations. More UV-LED research is expected, particularly targeting the unsolved issues of determining the wavelength-dependent airborne microorganism UV rate constant, improving the LED lamp power output, and evaluating UV-LED performance for in-duct applications.

- The UV rate constant is a species-dependent property of microorganisms upon UV irradiation. Although humidity has long been identified as a critical parameter affecting the UV rate constant, no general conclusion has been drawn due to the mixed influence reported in the literature. Radiation attenuation due to water layer absorption and UV light scattering of hygroscopic particles are the two potential reasons for the UV rate constant variations. However, further studies are needed to quantify these effects on microorganism disinfection.
- In this review, various in-duct UVGI system designs are summarized with the reported UV dose and overall system inactivation efficiency tabulated (Table 2). Further, the UVGI system design optimizations from the simulation results are presented in Table 3. The UV dose distribution in particle counts obtained by CFD simulations provides insight into the inactivation of individual bioaerosols. There is some degree of uncertainty about using the system's overall average UV dose to evaluate the inactivation efficiency owing to the presence of overdosed and underexposed particles. This observation highlights the need to consider the individual particle inactivation performance in addition to the overall system disinfection evaluation.
- In-duct UVGI system energy consumption predictions are discussed using the lamp output, meteorological climate, and installation locations in the HVAC system [17,18,83]. Based on previous studies, this paper introduces the humidity-amended UV rate constants and evaluates the corresponding energy consumptions under the monthly average environmental conditions for three meteorological climates. However, only the effect of humidity on the UV rate constant is quantified, but the influence of humidity on radiation transport and humidifier energy consumption is not discussed, which requires further study.
- Ultimately, to mitigate the COVID-19 transmission, this paper summarizes the in-duct UVGI designs in the literature and predicts their SARS-CoV-2 inactivation efficiencies (Tables 2 and 5) and energy consumption (Table 5). Two energy-efficient UVGI system designs (Designs #4 and #7) are identified as references for the UVGI design during the COVID-19 pandemic.

Declaration of competing interest

The authors declare that they have no known competing financial interests or personal relationships that could have appeared to influence the work reported in this paper.

Acknowledgements

The authors gratefully acknowledge the funding provided by the Natural Sciences and Engineering Research Council of Canada (NSERC) through the Alliance COVID-19 Grant and Canadian Institutes of Health Research (CIHR) and Alberta Innovates (AI) through Operating Grant: Canadian 2019 Novel Coronavirus (COVID-19) Rapid Research Funding Opportunity.

Appendix A. Supplementary data

Supplementary data to this article can be found online at https://doi.org/10.1016/j.buildenv.2021.107852.

References

[1] A.C. Fears, W.B. Klimstra, P. Duprex, A. Hartman, S.C. Weaver, K.S. Plante, D. Mirchandani, J. Plante, P.V. Aguilar, D. Fernandez, A. Nalca, A. Totura, D. Dyer, B. Kearney, M. Lackemeyer, J.K. Bohannon, R. Johnson, R.F. Garry, D.S. Reed, C. J. Roy, Comparative dynamic aerosol efficiencies of three emergent coronaviruses and the unusual persistence of SARS-CoV-2 in aerosol suspensions,, MedRxiv (2020), https://doi.org/10.1101/2020.04.13.20063784.

[2] J.L. Santarpia, D.N. Rivera, V. Herrera, M.J. Morwitzer, H. Creager, G. W. Santarpia, K.K. Crown, D. Brett-Major, E. Schnaubelt, M.J. Broadhurst, J. V Lawler, S.P. Reid, J.J. Lowe, Transmission potential of SARS-CoV-2 in viral shedding observed at the university of Nebraska medical center, 2020, https://doi.org/10.1101/2020.03.23.20039446. MedRxiv.

[3] P.Y. Chia, K.K. Coleman, Y.K. Tan, S.W.X. Ong, M. Gum, S.K. Lau, S. Sutjipto, P. H. Lee, T.T. Son, B.E. Young, D.K. Milton, G.C. Gray, S. Schuster, T. Barkham, P. P. De, S. Vasoo, M. Chan, B.S.P. Ang, B.H. Tan, Y.S. Leo, O.-T. Ng, M.S.Y. Wong, K. Marimuthu, Detection of air and surface contamination by severe acute respiratory syndrome coronavirus 2 (SARS-CoV-2) in hospital rooms of infected patients, MedRxiv (2020), https://doi.org/10.1101/2020.03.29.20046557.

[4] Y. Liu, Z. Ning, Y. Chen, M. Guo, Y. Liu, N.K. Gali, L. Sun, Y. Duan, J. Cai, D. Westerdahl, X. Liu, K. Xu, K. Ho, H. Kan, Q. Fu, K. Lan, Aerodynamic analysis of SARS-CoV-2 in two Wuhan hospitals, Nature (2020), https://doi.org/10.1038/s41586-020-2271-3.

[5] Z. Ding, H. Qian, B. Xu, Y. Huang, T. Miao, H.-L. Yen, S. Xiao, L. Cui, X. Wu, W. Shao, Y. Song, L. Sha, L. Zhou, Y. Xu, B. Zhu, Y. Li, Toilets dominate environmental detection of SARS-CoV-2 virus in a hospital, MedRxiv (2020), https://doi.org/10.1101/2020.04.03.20052175.

[6] R.T.7 Members, The ventilation of buildings and other mitigating measures for COVID-19: a focus on winter 2020, 1–62, http://arxiv.org/abs/2009.12781, 2020.

[7] P.W. Francisco, S.J. Emmerich, ASHRAE Position Document on Unvented Combustion Devices Approved by ASHRAE Board of Directors, Ashrae Stand, 2020.

[8] D.T. Stevens, P. Francisco, S.J. Emmerich, D.A. Baylon, T.M. Brennan, R. R. Crawford, D.C. Delaquila, L.L. Delaura, S.C. Drumheller, P.W. Fairey, D. H. Heberer, R.L. Hedrick, T.P. Heidel, M.C. Jackson, D.E. Jacobs, G.P. Langan, J. W. Lstiburek, J. Malone, S.I. Mason, J.C. Moore, A.B. Musser, J.P. Proctor, P. H. Raymer, M.H. Sherman, I.S. Walker, E.D. Werling, C.S. Barnaby, ASHRAE 62.1 Ventilation and Acceptable Indoor Air Quality, 2019, p. 58, 2019.

[9] S.E. Beck, R.A. Rodriguez, M.A. Hawkins, T.M. Hargy, T.C. Larason, K.G. Linden, Comparison of UV-induced inactivation and RNA damage in MS2 phage across the germicidal UV spectrum, Appl. Environ. Microbiol. 82 (2016) 1468–1474, https://doi.org/10.1128/AEM.02773-15.

[10] W. Kowalski, Ultraviolet Germicidal Irradiation Handbook, 2009, https://doi.org/10.1007/978-3-642-01999-9.

[11] P. Wargocki, Filtration and air cleaning, ASHRAE J. (2015).

[12] L. Sehulster, R.Y.W. Chinn, Guidelines for environmental infection control in health-care facilities, Morb. Mortal. Wkly. Rep. (2003).

[13] H. Sachs, S. Nadel, J.T. Amann, M. Tuazon, E. Mendelsohn, Emerging energy-saving technologies and practices for the buildings sector as of 2004, Am. Counc. … (2004).

[14] W.J. Kowalski, W.P. Bahnfleth, UVGI Design basics for air and surface disinfection, HPAC Heating, Piping, AirConditioning Eng. (2000).

[15] D. De Robles, S.W. Kramer, Improving indoor air quality through the use of ultraviolet technology in commercial buildings, Procedia Eng., 2017, https://doi.org/10.1016/j.proeng.2017.08.021.

[16] MarketsandMarkets, UV disinfection equipment market with COVID-19 impact analysis by component (UV lamps, reactor chambers), power rating (high, medium, low), application (water and wastewater, surface), end-user (municipal, residential), geography - global forecast to 2026. https://www.marketsandmarkets.com/Market-Reports/uv-disinfection-market-217291665.html, 2021.

[17] W. Bahnfleth, B. Lee, J. Lau, J. Freihaut, ANNUAL SIMULATION of IN-DUCT ULTRAVIOLET GERMICIDAL IRRADIATION SYSTEM PERFORMANCE William Bahnfleth , Bruno Lee , Josephine Lau , and James Freihaut Indoor Environment Center, Department of Architectural Engineering , The Pennsylvania State University, Design, 2009, pp. 1151–1158.

[18] B. Lee, W. Bahnfleth, K. Auer, Life-cycle cost simulation of in-duct ultraviolet germicidal irradiation systems, IBPSA 2009 - Int. Build. Perform. Simul. Assoc. (2009) 1159–1166, 2009.

[19] Y. Yang, H. Zhang, S.S. Nunayon, V. Chan, A.C.K. Lai, Disinfection efficacy of ultraviolet germicidal irradiation on airborne bacteria in ventilation ducts, Indoor Air 28 (2018) 806–817, https://doi.org/10.1111/ina.12504.

[20] A.J. Capetillo, Computational Fluid Dynamic Modeling of In-Duct UV Air Sterilisation Systems, 2015. http://etheses.whiterose.ac.uk/9591/.

[21] Food and Drug Administration (FDA), Ultraviolet Radiation for the Processing and Treatment of Food, 2011, pp. 24–27.

[22] U.V. Philips, Purification - Application Information, vol. 39, 2005. http://www.philps.com/uvpurification.

[23] J. Lau, W. Bahnfleth, J. Freihaut, Estimating the effects of ambient conditions on the performance of UVGI air cleaners, Build. Environ. 44 (2009) 1362–1370, https://doi.org/10.1016/j.buildenv.2008.05.015.

[24] H. Zhang, X. Jin, S.S. Nunayon, A.C.K. Lai, Disinfection by in-duct ultraviolet lamps under different environmental conditions in turbulent airflows, Indoor Air 30 (2020) 500–511, https://doi.org/10.1111/ina.12642.

[25] D. VanOsdell, K. Foarde, Defining the effectiveness of UV lamps installed in circulating air ductwork, prep. Air-conditioning refrig. Technol. Inst. Under ARTI 21-CR progr. Contract number 610-40030, Public from U.S. Dep. Commer. Natl. Tech. Inf. Serv. 5285 Port R. Road (2002). Springfie, Available to.

[26] V.T. Morgan, The overall convective heat transfer from smooth circular cylinders, Adv. Heat Tran. (1975), https://doi.org/10.1016/S0065-2717(08)70075-3.
[27] S.W. Churchill, M. Bernstein, A correlating equation for forced convection from gases and liquids to a circular cylinder in crossflow, J. Heat Tran. (1977), https://doi.org/10.1115/1.3450685.
[28] J. Taborek, Heat transfer of a cylinder in crossflow, Int. J. Heat Fluid Flow (1986), https://doi.org/10.1016/0142-727x(86)90066-4.
[29] EPA, Biological inactivation efficiency by HVAC in-duct ultraviolet light. UltraViolet Devices, Inc. Altru-V V-Flex (2006). Epa 600/R-06/049.
[30] EPA, Biological inactivation efficiency by HVAC in-duct ultraviolet light systems. Dust free bio-fighter 4Xtreme, Model 21 (2006). Epa 600/R-06/050.
[31] EPA, Biological inactivation efficiency by HVAC in-duct ultraviolet light systems, Atlantic Ultraviolet Corporation AeroLogic Model AD24-4 (2006). Epa 600/R-06/051.
[32] EPA, Biological inactivation efficiency by HVAC in-duct ultraviolet light, Steril-Aire, Inc. Model SE 1VO with GTS 24 VO emitter (2006). Epa 600/R-06/052.
[33] EPA, Biological inactivation efficiency by HVAC in-duct ultraviolet light systems, Sanuvox Technologies Inc. UV Bio-Wall 50 Outwardly Projecting Air Purifier (2006). Epa 600/R-06/053.
[34] EPA, Biological inactivation efficiency by HVAC in-duct ultraviolet light, American Ultraviolet Corporation ACP-24/HO-4 (2006). Epa 600/R-06/054.
[35] EPA, Biological inactivation efficiency by HVAC in-duct ultraviolet light, Novatron, Inc. BioProtector BP114i (2006). Epa/600/R-06/084.
[36] EPA, Biological inactivation efficiency by HVAC in-duct ultraviolet light systems, Abracair, LLC In-Duct System (2006). EPA 600/R-06/085.
[37] S.S. Nunayon, H. Zhang, A.C.K. Lai, Comparison of disinfection performance of UVC-LED and conventional upper-room UVGI systems, Indoor Air 30 (2020) 180–191, https://doi.org/10.1111/ina.12619.
[38] J.Y. Shin, S.J. Kim, D.K. Kim, D.H. Kang, Fundamental characteristics of deep-UV light-emitting diodes and their application to control foodborne pathogens, Appl. Environ. Microbiol. (2016), https://doi.org/10.1128/AEM.01186-15.
[39] S.S. Nunayon, H.H. Zhang, A.C.K. Lai, A novel upper-room UVC-LED irradiation system for disinfection of indoor bioaerosols under different operating and airflow conditions, J. Hazard Mater. 396 (2020) 122715, https://doi.org/10.1016/j.jhazmat.2020.122715.
[40] D. Kim, D. Kang, crossm UVC LED Irradiation Effectively Inactivates Aerosolized Viruses 84 (2018) 1–11.
[41] T. Koutchma, V. Popović, UV light-emitting diodes (LEDs) and food safety, Ultrav. LED Technol, Food Appl. From Farms to Kitchens (2019) 91–117, https://doi.org/10.1016/B978-0-12-817794-5.00005-4.
[42] J. Simonet, C. Gantzer, Inactivation of poliovirus 1 and F-specific RNA phages and degradation of their genomes by UV irradiation at 254 nanometers, Appl. Environ. Microbiol. (2006), https://doi.org/10.1128/AEM.01106-06.
[43] A. Bianco, M. Biasin, G. Pareschi, A. Cavalleri, C. Cavatorta, F. Fenizia, P. Galli, L. Lessio, M. Lualdi, E. Redaelli, I. Saulle, D. Trabattoni, A. Zanutta, M. Clerici, UV-C irradiation is highly effective in inactivating and inhibiting SARS-CoV-2 replication, SSRN Electron. J. (2020) 1–9, https://doi.org/10.2139/ssrn.3620830.
[44] C.S. Heilingloh, U.W. Aufderhorst, L. Schipper, U. Dittmer, O. Witzke, D. Yang, X. Zheng, K. Sutter, M. Trilling, M. Alt, E. Steinmann, A. Krawczyk, Susceptibility of SARS-CoV-2 to UV irradiation, Am. J. Infect. Contr. (2020), https://doi.org/10.1016/j.ajic.2020.07.031.
[45] H. Inagaki, A. Saito, H. Sugiyama, T. Okabayashi, S. Fujimoto, Rapid inactivation of SARS-CoV-2 with Deep-UV LED irradiation, Emerg. Microb. Infect. (2020) 1–8, https://doi.org/10.1080/22221751.2020.1796529.
[46] E.I. Patterson, T. Prince, E.R. Anderson, A. Casas-Sanchez, S.L. Smith, C. Cansado-Utrilla, T. Solomon, M.J. Griffiths, Á. Acosta-Serrano, L. Turtle, G.L. Hughes, Methods of inactivation of SARS-CoV-2 for downstream biological assays, J. Infect. Dis. (2020), https://doi.org/10.1093/infdis/jiaa507.
[47] H. Kariwa, N. Fujii, I. Takashima, Inactivation of SARS coronavirus by means of povidone-iodine, physical conditions and chemical reagents, Dermatology 212 (2006) 119–123, https://doi.org/10.1159/000089211.
[48] S.M. Duan, X.S. Zhao, R.F. Wen, J.J. Huang, G.H. Pi, S.X. Zhang, J. Han, S.L. Bi, L. Ruan, X.P. Dong, Stability of SARS coronavirus in human specimens and environment and its sensitivity to heating and UV irradiation, Biomed. Environ. Sci. 16 (2003) 246–255.
[49] M.E.R. Darnell, K. Subbarao, S.M. Feinstone, D.R. Taylor, Inactivation of the coronavirus that induces severe acute respiratory syndrome, SARS-CoV, J. Virol Methods (2004), https://doi.org/10.1016/j.jviromet.2004.06.006.
[50] M.E.R. Darnell, D.R. Taylor, Evaluation of inactivation methods for severe acute respiratory syndrome coronavirus in noncellular blood products, Transfusion 46 (2006) 1770–1777, https://doi.org/10.1111/j.1537-2995.2006.00976.x.
[51] B. Heimbuch, D. Harnish, ARA Research to Mitigate a Shortage of Respiratory Protection Devices during Public Health Emergencies, 2019. https://www.ara.com/news/ara-research-mitigate-shortage-respiratory-protection-devices-during-public-health-emergencies.
[52] M. Eickmann, U. Gravemann, W. Handke, F. Tolksdorf, S. Reichenberg, T. H. Mueller, A. Seltsam, Inactivation of three emerging viruses - severe acute respiratory syndrome coronavirus, Crimean-Congo haemorrhagic fever virus and Nipah virus - in platelet concentrates by ultraviolet C light and in plasma by methylene blue plus visible light, Vox Sang. (2020), https://doi.org/10.1111/vox.12888.
[53] M. Eickmann, U. Gravemann, W. Handke, F. Tolksdorf, S. Reichenberg, T. H. Müller, A. Seltsam, Inactivation of Ebola virus and Middle East respiratory syndrome coronavirus in platelet concentrates and plasma by ultraviolet C light and methylene blue plus visible light, respectively, Transfusion 58 (2018) 2202–2207, https://doi.org/10.1111/trf.14652.
[54] M. Saknimit, I. Inatsuki, Y. Sugiyama, K. Yagami, Virucidal efficacy of physico-chemical treatments against coronaviruses and parvoviruses of laboratory animals, Jikken Dobutsu 37 (1988) 341–345, https://doi.org/10.1538/expanim1978.37.3_341.
[55] Y. Liu, Y. Cai, X. Zhang, Induction of caspase-dependent apoptosis in cultured rat oligodendrocytes by murine coronavirus is mediated during cell entry and does not require virus replication, J. Virol. 77 (2003) 11952–11963, https://doi.org/10.1128/jvi.77.22.11952-11963.2003.
[56] M. Buonanno, D. Welch, I. Shuryak, D.J. Brenner, Far-UVC light (222 nm) efficiently and safely inactivates airborne human coronaviruses, Sci. Rep. 10 (2020) 1–8, https://doi.org/10.1038/s41598-020-67211-2.
[57] C.M. Walker, G. Ko, Effect of ultraviolet germicidal irradiation on viral aerosols, Environ. Sci. Technol. 41 (2007) 5460–5465, https://doi.org/10.1021/es070056u.
[58] N. Petrosillo, G. Viceconte, O. Ergonul, G. Ippolito, E. Petersen, COVID-19, SARS and MERS: are they closely related? Clin. Microbiol. Infect. (2020) https://doi.org/10.1016/j.cmi.2020.03.026.
[59] D.X. Liu, J.Q. Liang, T.S. Fung, Human coronavirus-229e, -OC43, -NL63, and -HKU1, Ref. Modul. Life Sci. (2020), https://doi.org/10.1016/b978-0-12-809633-8.21501-x.
[60] A. Wu, Y. Peng, B. Huang, X. Ding, X. Wang, P. Niu, J. Meng, Z. Zhu, Z. Zhang, J. Wang, J. Sheng, L. Quan, Z. Xia, W. Tan, G. Cheng, T. Jiang, Genome composition and divergence of the novel coronavirus (2019-nCoV) originating in China, Cell Host Microbe (2020), https://doi.org/10.1016/j.chom.2020.02.001.
[61] D. Benvenuto, M. Giovanetti, A. Ciccozzi, S. Spoto, S. Angeletti, M. Ciccozzi, The 2019-new coronavirus epidemic: evidence for virus evolution, J. Med. Virol. (2020), https://doi.org/10.1002/jmv.25688.
[62] J.F.W. Chan, S. Yuan, K.H. Kok, K.K.W. To, H. Chu, J. Yang, F. Xing, J. Liu, C.C. Y. Yip, R.W.S. Poon, H.W. Tsoi, S.K.F. Lo, K.H. Chan, V.K.M. Poon, W.M. Chan, J. D. Ip, J.P. Cai, V.C.C. Cheng, H. Chen, C.K.M. Hui, K.Y. Yuen, A familial cluster of pneumonia associated with the 2019 novel coronavirus indicating person-to-person transmission: a study of a family cluster, Lancet (2020), https://doi.org/10.1016/S0140-6736(20)30154-9.
[63] C.B. Beggs, E.J. Avital, Upper-room ultraviolet air disinfection might help to reduce COVID-19 transmission in buildings: a feasibility study, PeerJ (2020), https://doi.org/10.7717/peerj.10196.
[64] A.E. Gorbalenya, S.C. Baker, R.S. Baric, R.J. de Groot, C. Drosten, A.A. Gulyaeva, B. L. Haagmans, C. Lauber, A.M. Leontovich, B.W. Neuman, D. Penzar, S. Perlman, L. L.M. Poon, D.V. Samborskiy, I.A. Sidorov, I. Sola, J. Ziebuhr, The species Severe acute respiratory syndrome-related coronavirus: classifying 2019-nCoV and naming it SARS-CoV-2, Nat. Microbiol. 5 (2020) 536–544, https://doi.org/10.1038/s41564-020-0695-z.
[65] S. Ghimire, M. Flury, E.J. Scheenstra, C.A. Miles, Decay of SARS-CoV-2 and surrogate murine hepatitis virus RNA in untreated wastewater to inform application in wastewater-based epidemiology, Sci. Total Environ. (2019) 135577, https://doi.org/10.1016/j.scitotenv.2019.135577.
[66] Y. Ye, R.M. Ellenberg, K.E. Graham, K.R. Wigginton, Survivability, partitioning, and recovery of enveloped viruses in untreated municipal wastewater, Environ. Sci. Technol. (2016), https://doi.org/10.1021/acs.est.6b00876.
[67] J. Lau, W. Bahnfleth, R. Mistrick, D. Kompare, Ultraviolet irradiance measurement and modeling for evaluating the effectiveness of in-duct ultraviolet germicidal irradiation devices, HVAC R Res. 18 (2012) 626–642, https://doi.org/10.1080/10789669.2011.611575.
[68] J.I. Pearce-Walker, D.J. Troup, R. Ives, L.A. Ikner, J.B. Rose, M.A. Kennedy, M. P. Verhougstraete, Investigation of the effects of an ultraviolet germicidal irradiation system on concentrations of aerosolized surrogates for common veterinary pathogens, Am. J. Vet. Res. 81 (2020) 506–513, https://doi.org/10.2460/ajvr.81.6.506.
[69] M.D. Corbat, K. Owen, T.A. Mcgrath, R.B. Burkhead, D.M. Feddersen, C. Fischer, P. Maybee, S.W. Nicholas, C.Q. Sun, R.M. Harrold, S.J. Emmerich, J.D. Aswegan, K. I. Emerson, J.M. Ferguson, M.W. Gallagher, W.T. Grondzik, S.S. Hanson, R. L. Hedrick, Method of testing general ventilation air-cleaning devices for removal efficiency by particle size, ASHRAE Stand (2017) 1–64, 2007.
[70] H. Luo, L. Zhong, G. Zhang, An Improved Numerical Model of a UV-PCO Reactor for Air Purification Applications, 2020.
[71] S.A. Cuevas, C.A. Arancibia-Bulnes, B. Serrano, Radiation field in an annular photocatalytic reactor by the P1 approximation, Int. J. Chem. React. Eng. 5 (2007), https://doi.org/10.2202/1542-6580.1589.
[72] H. Einaga, J. Tokura, Y. Teraoka, K. Ito, Kinetic analysis of TiO2-catalyzed heterogeneous photocatalytic oxidation of ethylene using computational fluid dynamics, Chem. Eng. J. (2015), https://doi.org/10.1016/j.cej.2014.11.017.
[73] F. Denny, J. Scott, V. Pareek, G. Ding Peng, R. Amal, CFD modelling for a TiO2-coated glass-bead photoreactor irradiated by optical fibres: photocatalytic degradation of oxalic acid, Chem. Eng. Sci. (2009), https://doi.org/10.1016/j.ces.2008.12.021.
[74] F.J. Trujillo, T. Safinski, A.A. Adesina, Oxidative photomineralization of dichloroacetic acid in an externally-irradiated rectangular bubble tank reactor: computational fluid dynamics modeling and experimental verification studies, Ind. Eng. Chem. Res. (2010), https://doi.org/10.1021/ie901364z.
[75] J.E. Duran, M. Mohseni, F. Taghipour, Computational fluid dynamics modeling of immobilized photocatalytic reactors for water treatment, AIChE J. (2011), https://doi.org/10.1002/aic.12399.
[76] P. Atkins, J. De Paula, Atkins' Physical Chemistry, Chemistry (2009), https://doi.org/10.1021/ed056pA260.1 eighth ed.
[77] ANSYS Academic Research, ANSYS Fluent Theory Guide, ANSYS Help Syst., 2018.

[78] A. Capetillo, C.J. Noakes, P.A. Sleigh, Computational fluid dynamics analysis to assess performance variability of in-duct UV-C systems, Sci. Technol. Built Environ. 21 (2015) 45–53, https://doi.org/10.1080/10789669.2014.968512.
[79] F. Atci, Y.E. Cetin, M. Avci, O. Aydin, Evaluation of in-duct UV-C lamp array on air disinfection: a numerical analysis, Sci. Technol. Built Environ. 4731 (2020), https://doi.org/10.1080/23744731.2020.1776549.
[80] A. Capetillo, C.J. Noakes, P.A. Sleigh, A. Khan, In-duct uvgi air sterilisation: optimisation study for high performance energy efficient systems, in: Indoor Air 2014 - 13th Int. Conf. Indoor Air Qual. Clim., 2014, pp. 594–599.
[81] A.J. Capetillo, Computational Fluid Dynamic Modeling of In-Duct UV Air Sterilisation Systems, 2015.
[82] C.H. Thatcher, B.R. Adams, Impact of surface reflection on microbial inactivation in a UV LED treatment duct, Chem. Eng. Sci. (2020) 116204, https://doi.org/10.1016/j.ces.2020.116204.
[83] B. Lee, W.P. Bahneth, Effects of installation location on performance and economics of in-duct ultraviolet germicidal irradiation systems for air disinfection, Build. Environ. 67 (2013) 193–201, https://doi.org/10.1016/j.buildenv.2013.05.019.
[84] D.G. Sharp, The effects of ultraviolet light on bacteria suspended in air, J. Bacteriol. (1940), https://doi.org/10.1128/jb.39.5.535-547.1940.
[85] C.W. Chang, S.Y. Li, S.H. Huang, C.K. Huang, Y.Y. Chen, C.C. Chen, Effects of ultraviolet germicidal irradiation and swirling motion on airborne Staphylococcus aureus, Pseudomonas aeruginosa and Legionella pneumophila under various relative humidities, Indoor Air 23 (2013) 74–84, https://doi.org/10.1111/j.1600-0668.2012.00793.x.
[86] ASHRAE-55, Thermal environmental conditions for human occupancy, ANSI/ASHRAE Stand. - (2017) 55.
[87] Health Canada, RELATIVE HUMIDITY INDOORS, FACTSHEET, 2016, pp. 1–3.
[88] C.C. Tseng, C.S. Li, Inactivation of virus-containing aerosols by ultraviolet germicidal irradiation, Aerosol Sci. Technol. 39 (2005) 1136–1142, https://doi.org/10.1080/02786820500428575.